Journal of Applied Polymer Science

# Effects of nano-$TiO_2$ on the performance of high-amylose starch based antibacterial films

**Chao Liu, Hanguo Xiong, Xing Chen, Shun Lin, Yanhua Tu**
College of Food Science and Technology, Huazhong Agricultural University, Wuhan 430070, China
Correspondence to: Hanguo Xiong (E-mail: xionghanguo@163.com)

**ABSTRACT:** The purpose of this article is to investigate the effects of nano-tianium dioxide (nano-$TiO_2$) on the high-amylose starch/polyvingl alcohol (PVA) blend films prepared by a solution casting method. The results show that at the concentration of 0.6% of nano-$TiO_2$, the film demonstrated the best tensile strength at 9.53 MPa, and the elongation at break was noted as 49.50%. The optical *transmittance* of the film was decreased and the water resistance was improved with further increase of the concentration of nano-$TiO_2$. Using the techniques of Fourier transform infrared spectroscopy (FTIR), differential scanning calorimetry (DSC), and field-emission scanning electron microscopy (SEM), the molecular and the crystal structures of the films were characterized. The results indicate that the miscibility and compatibility between high-amylose starch and PVA were increased with the addition of nano-$TiO_2$ into the films due to the formation of hydrogen and C—O—Ti bonds. The antimicrobial activities of the blend films were also explored. The results show that there were inhibitory zones around the circular film disc, which is attributable to the addition of nano-$TiO_2$. © 2015 Wiley Periodicals, Inc. J. Appl. Polym. Sci. **2015**, *132*, 42339.

**KEYWORDS:** biodegradable; blends; composites; films

Received 9 March 2015; accepted 10 April 2015
**DOI: 10.1002/app.42339**

## INTRODUCTION

In the food packaging industry, starch has been considered as a suitable source material for its inherent biodegradability, ready availability, and relatively low cost.[1,2] Corn starch films exhibit appropriate physical properties since these films are isotropic, odourless, tasteless, nontoxic, and biodegradable. However, the films made from corn starch are water sensitive and would present inferior mechanical properties compared with conventional plastic films. Previous reports show that properties of corn starch are different with different amylose content.[3] It is reported that the film has higher water resistance and better mechanical property with the increase of amylose content.[4]

Starch/polyvinyl alcohol (PVA) blend plastics are one of the most popular plastics, and are widely used in packaging and agricultural applications.[5,6] PVA has the advantages of good film formation, strong conglutination, and high thermal stability. In recent years, PVA has been more and more applied in the materials industry.[7,8] In addition, the molecular structures of the corn starch and PVA share some similarities. Therefore, the solution of corn starch gel mixed with PVA has been widely applied in binder, starch plastics, and other fields.[9]

$TiO_2$ is a kind of environmentally friendly material. Numerous studies have indicated that nanometer materials can improve the performance of polymer materials, including starch and nano-$SiO_2$.[10–13] However, relevant studies investigating antimicrobial properties in this film have not been reported regarding high-amylose polymers modified by nano-$TiO_2$. A Ti atom is connected to another Ti atom via bridging oxygen atoms and the total chemical composition is denoted as $TiO_2$. This structure results in the existence of unpaired electrons (dangling bonds) on the surface Ti or O atoms, and the quantity of dangling bonds is proportional to the surface atomic number and inversely proportional to the molecular size of nano-$TiO_2$.[14,15] Anatase nano-$TiO_2$,[16] which is an inorganic nanoparticle with large specific surface area and high surface energy, has been widely employed in the research and development of solar cell, sewage disposal, antibacterial materials, and self-cleaning materials because of its high photocatalytic activity.[17,18] In addition to these structures, several hydroxide radical groups and dangling bonds can be adsorbed on the surface of nano-$TiO_2$, which may remarkably affect the physical properties of natural polymers/thermoplastic films.[19]

Nano-$TiO_2$, as a good inorganic nanometer material, also has potential antibacterial activities compared with other nanomaterials. It is shown that nano-$TiO_2$ exhibits antibacterial activity under UV light irradiation due to the formation of various reactive oxygen species (ROS). And excess destructive ROS may

produce oxidative stress and attack membrane lipids, ultimately resulting in membrane or DNA damage.[20,21] Compared with organic materials, nano-$TiO_2$ has good chemical and thermal stability, and it does not result in drug resistance of bacteria. It is worth noting that $TiO_2$ has been approved by the American Food and Drug Administration (FDA) for use in human food and compounded in food contact materials.[22]

In this article, high-amylose starch was prepared by enzymolysis approach. The high-amylose starch/PVA blend films were prepared by a casting method, and nano-$TiO_2$ was used to improve the properties of the blend films. The effects of nano-$TiO_2$ on the structure and properties of the blend films were investigated.

## EXPERIMENTAL

### Materials

PVA was produced and provided by Chongqing Inorganic Chemical Reagent Factory (DP 2099 ± 50). High-amylose starch (amylose content about 50%) was obtained by enzymolysis approach. Nano-titanium dioxide (nano-$TiO_2$, 99.8%, 60 nm, anatase, Aladdin industrial corporation), glycerol, and sodium chloride of analytical grade were produced by Sinopharm Chemical reagent Co., Ltd. Nutrient agar was obtained from Qingdao Hope Bio-Technology Co., Ltd. Deionized water was obtained from Hangzhou Wahaha Group Co., Ltd.

### Preparation of the Films

Nano-$TiO_2$ high-amylose starch/PVA blend films were prepared by casting method. In this method, 10 g high-amylose starch was dissolved for 30 min in hot water (100 mL, 95°C); meanwhile, 6 g PVA was dissolved for 40 min in hot water (150 mL, 95°C). The gelatinized starch was mixed to homogeneously form gel solution at 95°C. Three grams of glycerol and nano-$TiO_2$ (0–1% of starch quality) were added to the above mixture with continuous stirring for 30 min on a magnetic stirrer (1500 rpm) at the same temperature. The solutions were then poured onto a glass plate. The cast solutions were allowed to dry at 50°C for 12 h. Then, the fully dried membranes were peeled away from the glass plate to get the product. The nano-$TiO_2$ content of the SPT0, SPT1, SPT2, SPT3, SPT4, and SPT5 was 0, 0.2, 0.4, 0.6, 0.8, and 1%, respectively.

### Mechanical Properties of the Films

The tensile strength and elongation at break of the films were measured on the electron tensile tester CMT-6104 according to Chinese standard method GB/T4456-96 (Polyethylene Blown film for packaging, 1996). The films were cut into 120 × 15 mm strips, with the gauge length set at 80 mm, a tensile rate of 250 mm/min, a return rate of 200 mm/min, and a breaking load of 200 N.

### Water Absorption

Dried films were immersed in distilled water at room temperature (25°C). After equilibrium (24 h), moisture on the surface of the film was removed, and the weight of the films was measured. The water absorption ($W_a$) in the film was calculated as follows:

$$W_a = (W_e - W_0)/W_0,$$

where $W_e$ is the weight of the film after soaking in water for 24 h at room temperature, and $W_0$ is the first dry weight of the film. The swelled films were dried again for 24 h at 60°C.

### Optical Transmittance

The transmittance of the film (0.15 mm thickness) was measured by using a Shimadzu UV-1700 spectrophotometer (Shimadzu, Kyoto, Japan) in the wavelength range of 400–800 nm. Film specimen was cut into a rectangle piece and placed in a spectrophotometer test cell directly, and air was used as reference.[23] Measurements were performed at least in three replicates.

### Antibacterial Activity

Antibacterial activities of SPT blend films were measured against Gram-negative (*Escherichia coli*) and Gram-positive bacteria (*Staphylococcus aureus*) with inhibition zone method.[24]

A suspension of 1.0 mL initial bacteria was taken into tube, and then was diluted to 10 mL with normal saline at a dilution factor of $10^{-1}$ (I). Then 1.0 mL solution in tube (I) was transplanted to tube, according to the same dilution process, and the dilution factor was $10^{-2}$ (II). Similarly, the dilution factor of tube (III) was $10^{-3}$.

Five milliliters of warm liquid culture medium (Nutrient agar) was put into a Petri dish. 0.25 mL bacteria dilution from tube (III) was added onto the surface of the solid culture medium after the Nutrient agar was cooled to ambient temperature, and then uniformly daubed with coating stick. The circular film (Ø8 mm) was attached onto the solid culture medium, and then the plates were incubated for 24 h at 37°C. Finally, the diameter of inhibition ring of film was measured, and the longer the diameter of inhibition ring of film is, the better the antibacterial effects are.

### Fourier Transform Infrared (FTIR) Spectroscopy

FTIR spectra of nano-$TiO_2$ high-amylose starch/PVA blend films were recorded on a Perkin-Elmer spectrophotometer using KBr pellets. The wave range, which was from 4000 to 400 $cm^{-1}$ with a resolution of 4 $cm^{-1}$, was scanned 32 times for spectrum integration.

### Differential Scanning Calorimeter (DSC)

The thermal properties of the blend films were determined by using a DSC 200PC (NETZSCH, Germany) under nitrogen atmosphere. The samples of 5–10 mg were encapsulated into aluminum pans and were heated from 298 to 523 K at a rate of 10 K/min, and then the temperature was kept at 523 K for 5 min to erase previous thermal history. Subsequently, the samples were cooled to 523 K at the rate of 10 K/min to obtain the crystallization curve and kept at this temperature for 2 min. Afterward, the samples were heated to 523 K at the rate of 10 K/min to obtain the melting curve.

### Scanning Electron Microscopy (SEM)

The surfaces and morphologies of nano-$TiO_2$ high-amylose starch/PVA composites were investigated by a Hitachi (Japan) S-4800 field emission scanning electron microscope (SEM).

## RESULTS AND DISCUSSION

### Mechanical Properties of the Films

The mechanical properties of the blend films are of great importance due to their influence on product performance. The

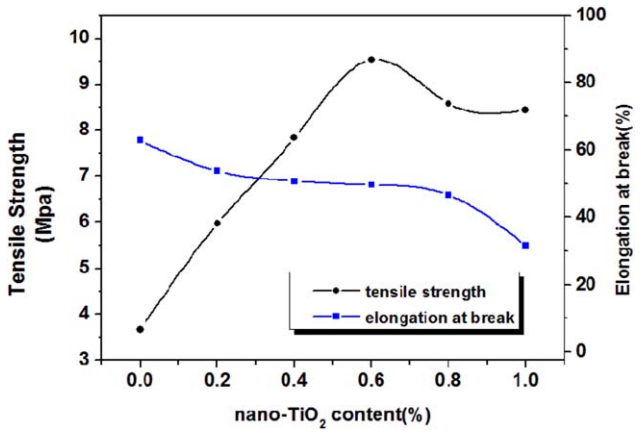


**Figure 1.** The tensile strength and break at elongation of SPT films. [Color figure can be viewed in the online issue, which is available at wileyonlinelibrary.com.]

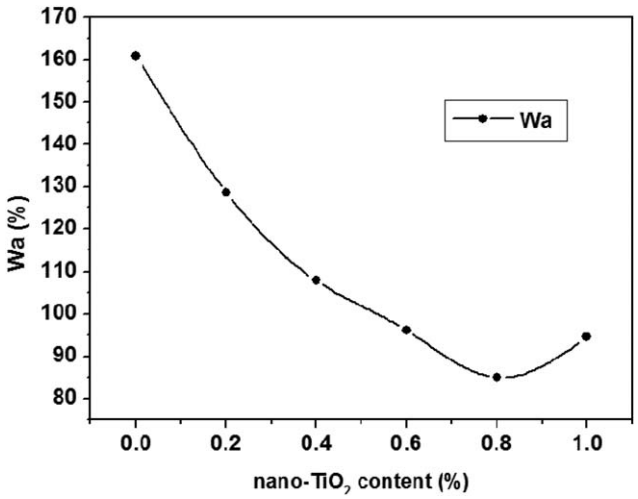


**Figure 2.** The water absorption of the SPT films.

dependence of the tensile strength on the nano-$TiO_2$ content of the blend films is shown in Figure 1. The tensile strength of the SPT0 film was 3.66 MPa. When the nano-$TiO_2$ content in the film was increased from 0 to 0.6%, the tensile strength of the film was increased by 160.38%, which amounted to 9.53 MPa. This phenomenon is because when nano-$TiO_2$ was added into the films, the intermolecular interfacial adhesion and the molecular chain rigidity of high-amylose starch/PVA were enhanced with the existence of hydrogen and covalent bonds between nano-$TiO_2$ and high-amylose starch/PVA results from nano-$TiO_2$, which remarkably improved the tensile strength of the blend films. When the nano-$TiO_2$ content exceeded 0.6%, the tensile strength of the blend films showed a slight decline along with an increase of nano-$TiO_2$ content, but it was still much higher than that of SPT0. In general, nanoparticles being very small in size (<100 nm) have great tendency for agglomeration to minimize surface to volume ratio and, in turn, the surface free energy of the system,[24] so the slight decline results from this reason. The agglomeration of nano-$TiO_2$ reduces the quantity of nano-sized $TiO_2$ particle, and fewer nano-$TiO_2$ particles could enter the space between the high-amylose starch/PVA molecules to form new hydrogen and covalent bonds. Thus, the hydrogen and covalent bonds between nano-$TiO_2$ and high-amylose starch/PVA are reduced, and the positive influence of nano-$TiO_2$ is decreased. On the whole, the addition of nano-$TiO_2$ can significantly improve the performance of the blend films.

Unlike the tensile strength, the elongation at break of the blend films decreased slowly from 62.74 to 31.71% along with an increase of nano-$TiO_2$ content (Figure 1). As nano-$TiO_2$ enhanced the molecular chain rigidity with the help of hydrogen and covalent bonds, the molecular chain elasticity was receded, when the pulling force is large enough, the molecular chain fracture directly without too much deformation. Thus, nano-$TiO_2$ decreased the elongation at break of the films.

### Water Absorption

Water absorption of the films is shown in Figure 2. It can be seen that the water absorption of the blend films decreased with an increase of nano-$TiO_2$ content in general. The water absorption of the SPT0 film was 160.92%, while SPT4 had the lowest water absorption at about 84.99%. The reason is that nano-$TiO_2$ was inserted into the space between the high-amylose starch/PVA molecules to form more hydrogen and covalent bonds, and the existence of these molecular links resulted in the molecular structure became more perfect and compact. This variation of microstructure can prevent the water molecules to enter, thereby further reducing the water dissolving, which improved the water resistance of the films. When the nano-$TiO_2$ content exceeded 0.8%, the water absorption of the films was increased from 84.99 to 94.60%, but it was still much lower than 160.92% of the SPT0 film. Similar to tensile strength, this rebound phenomenon can mainly be attributed to the same reason that when the concentration of nano-$TiO_2$ was increased, the agglomeration of nano-$TiO_2$ reduced the quantity of nano-sized $TiO_2$ particle, thus lead to the microstructure of the blend films which was not compact enough compared with SPT4, so

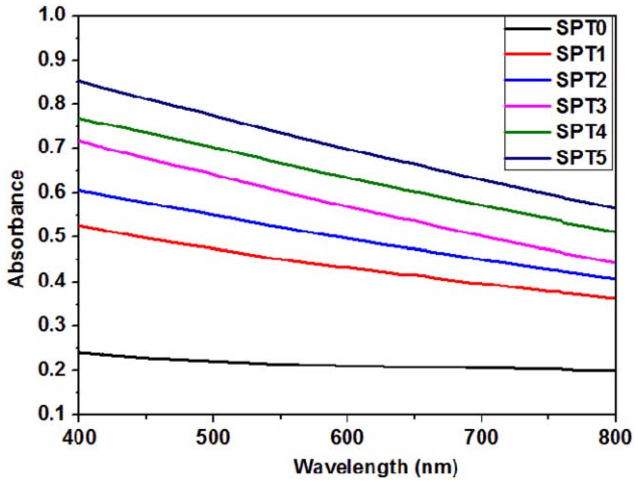


**Figure 3.** Absorbance of the SPT films over a wavelength range of 400–800 nm. [Color figure can be viewed in the online issue, which is available at wileyonlinelibrary.com.]

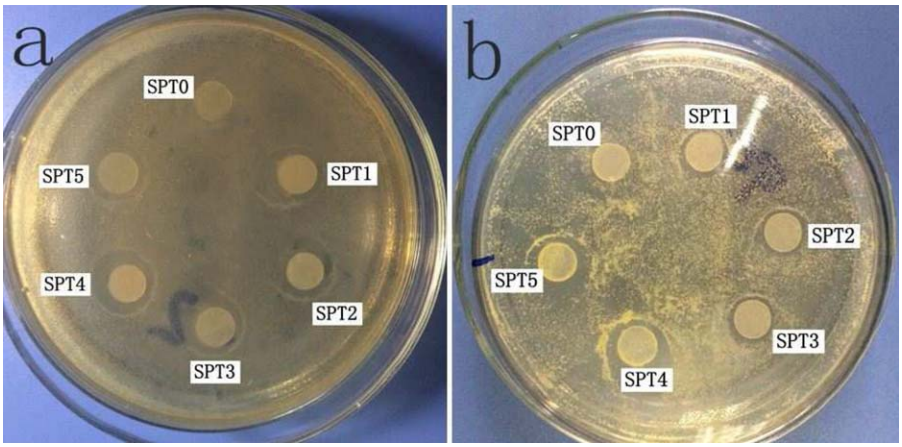


**Figure 4.** Inhibitory effect of SPT films against (a) *E. coli* and (b) *S. aureus*. [Color figure can be viewed in the online issue, which is available at wileyonlinelibrary.com.]

that some water molecules entered the space of blend films and dissolved it.

### Optical Transmittance of the Films

The optical transmittance of the films is shown in Figure 3. The overall absorbance of the blend films was increased with the increase of nano-$TiO_2$ content. As absorbance is inversely proportional to the transmittance; therefore, according to the figure, it can be concluded that the transmittance was sharply declined when nano-$TiO_2$ was added into the films. This result was mainly due to the characteristic of nano-$TiO_2$ itself which greatly facilitated the diffuse reflection of light. The diffuse reflection of light was easily occurred on the interface of nano-$TiO_2$, due to large specific surface area and high refractive index. Additionally, this characteristic did not change when it is added to the blend films, which consequently increased the light absorbance of the blend films.

The absorbance in the ultraviolet region was higher than that of infrared region in terms of variation tendency especially in the films with nano-$TiO_2$. This suggested that nano-$TiO_2$ tend to absorb ultraviolet light owing to the fact that short-wave light (ultraviolet) has more energy than long-wave light (infrared). So, nano-$TiO_2$ absorbed more ultraviolet which ultimately resulted into the occurrence of photocatalysis. Ultraviolet light is easier to result in rot of food. This characteristic of nano-$TiO_2$ to absorb ultraviolet and visible light has great potential application in preservation of food to avoid light.

### Antibacterial Activity Analysis

The nano-$TiO_2$ high-amylose starch/PVA blend films were screened for their antibacterial activities against Gram-positive (*S. aureus*) and Gram-negative (*E. coli*) bacteria. The inhibitory effect was measured based on clear zone surrounding circular film disc. Our measurement of inhibition zone diameter included the diameter of film disc; therefore, the values were always higher than that of the diameter of film disc. If there was no inhibitory zone, the diameter was valued as zero.

As shown in Figure 4, the films showed relative fair antibacterial activity against Gram-positive (*S. aureus*) and Gram-negative (*E. coli*) bacteria. Inhibition zone was observed for all the samples containing nano-$TiO_2$ except SPT0 films which were completely surrounded by bacterial colonies when placed in the two kinds of bacterial culture medium. The results of measurement of inhibitory zone against *S. aureus* and *E. coli* are shown in Table I. According to Table I, on the whole, with increase in nano-$TiO_2$ contents, the inhibition zone around the samples was increased from 10.24 to 13.34 mm for *E. coli* and 10.09 to 11.94 mm for *S. aureus* which showed that the antibacterial activity of nano-$TiO_2$ is better against *E. coli* as compared to *S. aureus*.

$TiO_2$ can generate strong oxidizing power when illuminated under ultraviolet (UV) light with wavelengths of $<385$ nm.[25] The photon energy generates an electron-hole pair on the $TiO_2$ surface. The hole in the valence band can then react with water or hydroxide ions adsorbed on the surface to produce hydroxyl radical ($OH^{\bullet}$), and the electrons in the conduction band can reduce $O_2$ to produce superoxide ions ($O_2^{-}$). It is very likely that both holes and $OH^{\bullet}$ attack membrane lipids, ultimately resulting in membrane or DNA damage. Thereby, $TiO_2$ can restrain the growth of the bacteria. Even so, with the incubation time going by, the inhibition zone will gradually disappear, suggesting that the bacteriostatic ability of nano-$TiO_2$ is not strong enough.

### FTIR Analysis

The FTIR spectra of the blend films are shown in Figure 5. According to Figure 5(a), the absorption peaks can be seen at 2921.13 and 1386.33 $cm^{-1}$, which was due to the stretching vibrations of the C—H and C—C, respectively. The bands due to the CH and $CH_2$ deformation vibrations were present at the

**Table I.** The Value of Inhibition Zones

| Sample | *E. coli* (mm) | *S. aureus* (mm) |
|---|---|---|
| SPT0 | 0 | 0 |
| SPT1 | 10.24 | 10.09 |
| SPT2 | 11.36 | 10.24 |
| SPT3 | 12.26 | 10.22 |
| SPT4 | 13.34 | 11.94 |
| SPT5 | 11.22 | 11.22 |

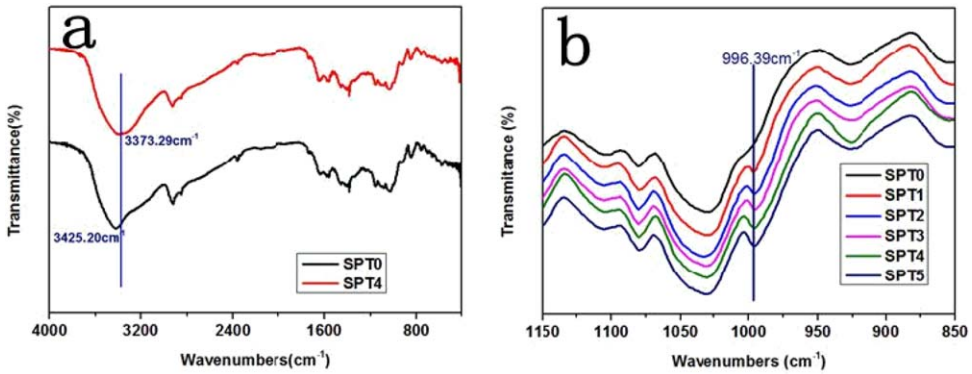


**Figure 5.** (a) FTIR spectra of SPT films at range of 400–4000 $cm^{-1}$ and (b) FTIR spectra of SPT films at range of 850–1150 $cm^{-1}$. [Color figure can be viewed in the online issue, which is available at wileyonlinelibrary.com.]

range of 1300–1500 $cm^{-1}$. The broad hydroxyl band, which is also very intensive, occurs at 3000–3600 $cm^{-1}$, and the peaks caused by an accompanying C—O stretching are present at 1000–1260 $cm^{-1}$. It was noteworthy that a broad and strong absorption around 3420 $cm^{-1}$ represents the characteristic absorption of the stretching vibration of —OH and the formation of hydrogen bonds among the —OH groups. Obviously, the absorption band of the —OH shifted to a lower wave number from 3425.20 to 3373.29 $cm^{-1}$ with the addition of nano-$TiO_2$. In general, the formation of hydrogen bonds reduces the force constant of the participants, thereby resulting in a red shift. Similarly, new hydrogen bonds were formed on the surface of nano-$TiO_2$ because the free —OH group combined with that of high-amylose starch/PVA which resulted in strong intermolecular hydrogen bonding.

The free —OH on the surface of nano-$TiO_2$ results in the formation of hydrogen bonds, beyond that, a large amount of unsaturated dangling bonds were on the surface of nano-$TiO_2$, these dangling bonds are conducive to form covalent bond. In our experiment, these dangling bonds could have covalent interactions with high-amylose starch/PVA composites, forming the bond of C—O—Ti. Figure 5(b) shows that the FTIR spectra of the films were at the range of 1150–800 $cm^{-1}$. SPT0 has no peak at the 996.39 $cm^{-1}$; while when the nano-$TiO_2$ content in the films was increased, the peak around 996.39 $cm^{-1}$ became increasingly evident compared with that of SPT0. This peak at 996.39 $cm^{-1}$ was attributed to the C—O—Ti group, which confirms the occurrence of covalent interactions between nano-$TiO_2$ and high-amylose starch or PVA.

### DSC Analysis

The role of nano-$TiO_2$ in modifying the crystallinity of PVA can be determined by using the DSC analysis. Figure 6 presents the DSC melting curves and crystallization degree of the blend films. The crystallization degree of the PVA component in the composites was determined by the melting peak area using the following equation:

$$X_c = (\Delta H_m / \varphi \Delta H^0{}_m) \times 100\%,$$

where $\triangle H_m$ is the enthalpy of fusion of the sample, $\triangle H^0{}_m$ is the heat of fusion for 100% crystalline PVA, and $\varphi$ is the weight fraction of PVA in the films. In this equation, $\triangle H_m$ is dependent on the peak area, and $\triangle H^0{}_m$ and $\varphi$ are constant. Therefore, the crystallization degree of the sample is in direct proportion to the peak area.

According to this principle, as shown in Figure 6, the peak area was reduced by 45.99% when the content of nano-$TiO_2$ was increased from 0 to 0.8%. The reduction in peak area can be illustrated by the fact that the number of cross-links was increased by adding nano-$TiO_2$ (as shown in FTIR analysis) which caused decrease in crystallinity degree. The formation of new hydrogen and covalent bonds disturb the parallel direction of the high-amylose starch/PVA chains and further restricts the molecular motion and rearrangement. Besides, the addition of nano-$TiO_2$ could strengthen the rigidity of high-amylose starch/PVA chain, which also hinders the crystallization of the films.

The DSC cooling thermogram and the crystallinity versus time for the crystallization of SPT films during the cooling crystallization process are plotted in Figure 7(a,b). The crystallization time of the PVA was determined using the following equation:

$$t = (T_0 - T)/\theta,$$

where $T_0$ is the initial crystallization temperature, $T$ is the crystallization temperature, and $\theta$ is the cooling rate (10 K/min).

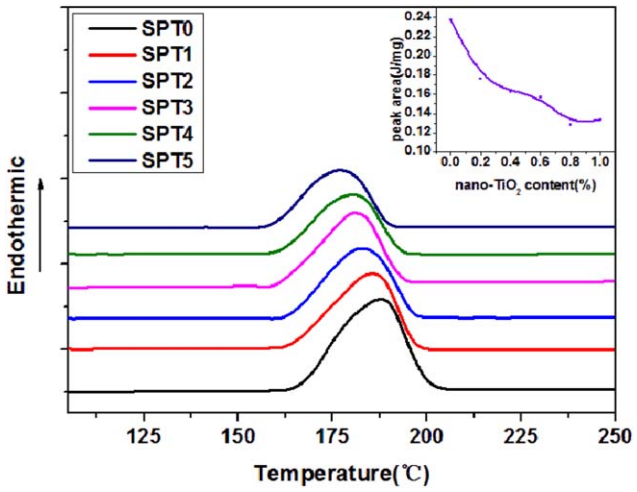


**Figure 6.** DSC melting curves of SPT films. [Color figure can be viewed in the online issue, which is available at wileyonlinelibrary.com.]

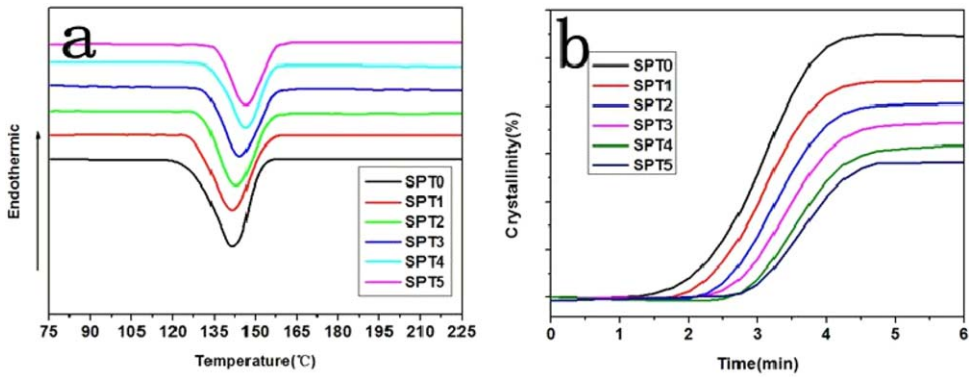


**Figure 7.** (a) DSC cooling thermograms and (b) plots of $X_c$ versus time for the crystallization of SPT films. [Color figure can be viewed in the online issue, which is available at wileyonlinelibrary.com.]

According to this equation, since $\theta$ is a constant, thus $t$ depends mainly on $T_0$, and the crystallization degree depends on the peak area.

In Figure 7(a), the initial crystallization temperature was delayed with the increase of nano-$TiO_2$ content; meanwhile, the DSC peak value was delayed too, and the peak area was decreased gradually. It can be speculated that the crystallization rate and degree were decreased substantially. In order to expound the conclusion more intuitively, it calculated the integral of Figure 7(a) to get Figure 7(b) according to FEI' analysis method.[14] In Figure 7(b), abscissa is the delay time, the ordinate is the peak area, $T_0$ delayed nearly 1.5 min, and the peak area declined distinctly, so, it can be concluded that the crystallization rate and degree were decreased, which was in accordance with the result that the addition of nano-$TiO_2$ hindered the crystallization of PVA.

**SEM Analysis**

The morphology of the blend films was characterized by FESEM, and the results are shown in Figure 8. The SPT4 films are more smooth and compact, while the SPT0 films has several irregular particles, suggesting that the miscibility and compatibility in each component in SPT4 films were increased. Because the surface of the nano-$TiO_2$ has plenty of unsaturated residual bonds and different hydroxyl group bonding states, it is easy to enter the space of high-amylose starch and PVA molecules and form a strong hydrogen bond or a strong chemical bond C—O—Ti with high-amylose starch and PVA, to further reduce the reunion of the same molecules. Hence, there was a strong interfacial binding force between nano-$TiO_2$ and high-amylose starch/PVA, and the film surface showed a compact and smooth microstructure. In fact, nano-$TiO_2$ plays the role of the cross-linking agent, which effectively improves the compatibility of

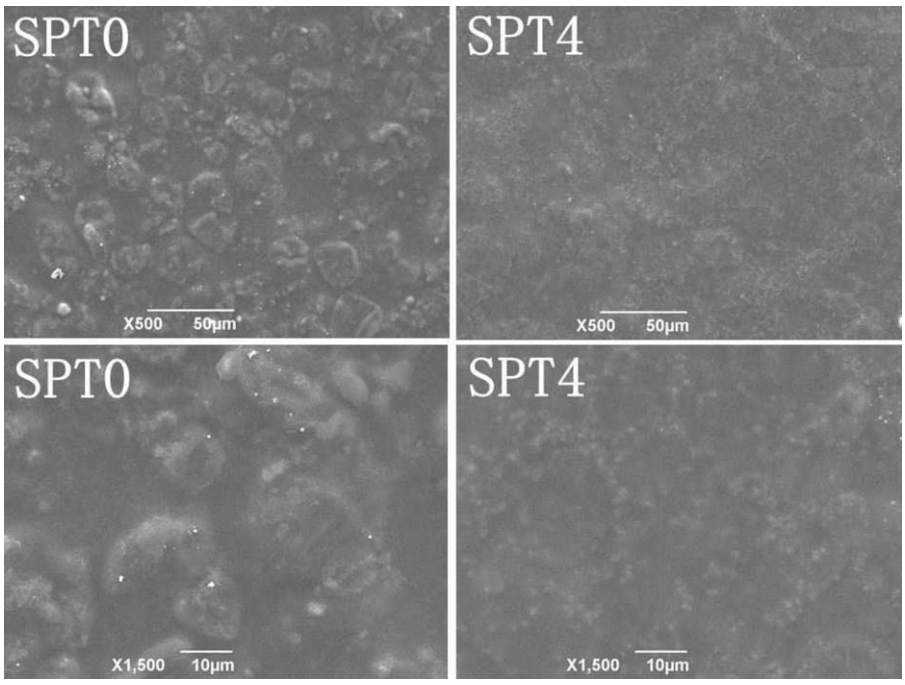


**Figure 8.** SEM micrographs of surfaces of SPT0 and SPT4 films.

high-amylose starch and PVA and makes the film surface and structure more smooth and dense.

## CONCLUSIONS

The findings of this study reveal that the properties of high-amylose starch/PVA blend films can be improved through the addition of nano-$TiO_2$. It also demonstrated that the miscibility and compatibility are increased between nano-$TiO_2$ and high-amylose starch/PVA due to the formation of hydrogen and C—O—Ti bonds, which greatly affects the characteristics of the blend films. The crystallization degree and rate as well as the optical transmittance of the blend films were decreased with the increase of nano-$TiO_2$ concentration. A significant improvement was observed in the mechanical properties and water resistance of the blend films. SPT3 exhibited the best tensile strength at 9.53 MPa together with a relatively better water resistance. Moreover, the addition of nano-$TiO_2$ obviously enhances the activity against the Gram-negative (*E. coli*) and Gram-positive (*S. aureus*) bacteria in the blend films. In conclusion, nano-$TiO_2$ high-amylose starch/PVA blend films have a great potential for food packaging applications.

## ACKNOWLEDGMENTS

The authors gratefully acknowledge the financial assistance supported by the National Natural Science Foundation of China (No. 31471699), the Fundamental Research Funds for the Central Universities (No. 2011PY152), and the "Twelfth Five-Year" National Science and Technology Support Program (No. 2012BAD54G01).

## REFERENCES

1. Xiong, H.; Tang, S.; Tang, H.; Zou, P. *Carbohyd. Polym.* **2008**, *71*(2), 263.
2. Mathew, S.; Abraham, T. E. *Food Hydrocolloids* **2008**, *22*(5), 826.
3. Matveev, Y. I.; Van Soest, J. J. G.; Nieman, C.; Wasserman, L. A.; Protserov, V. A.; Ezernitskaja, M.; Yuryev, V. P. *Carbohyd. Polym.* **2001**, *44*(2), 151.
4. Mondragon, M.; Mancilla, J. E.; Rodríguez-González, F. J. *Polym. Eng. Sci.* **2008**, *48*(7), 1261.
5. Priya, B.; Gupta, V. K.; Pathania, D.; Singha, A. S. *Carbohyd. Polym.* **2014**, *109*, 171.
6. Xiao, C.; Yang, M. *Carbohyd. Polym.* **2006**, *64*(1), 37.
7. Pereira Junior, V. A.; de Arruda, I. N. Q.; Stefani, R. *Food Hydrocolloids* **2015**, *43*, 180.
8. Halajan, M.; Torkamany, M. J.; Dorranian, D. *J. Phys. Chem. Solids* **2014**, *75*, 1187.
9. Shigang, L.; Peirong, C.; Suwen, Z. *J. Chin. Cereals Oils Assoc., Vo.* **2010**, l 25, (No.12).
10. Yao, K.; Cai, J.; Liu, M.; Yu, Y.; Xiong, H.; Tang, S.; Ding, S. *Carbohyd. Polym.* **2011**, *86*(4), 1784.
11. Tang, S.; Zou, P.; Xiong, H.; Tang, H. *Carbohyd. Polym.* **2008**, *72*(3), 521.
12. Slavutsky, A. M.; Bertuzzi, M. A. *Carbohyd. Polym.* **2012**, *90*(1), 551.
13. Tee, T. T.; Sin, L. T.; Gobinath, R.; Bee, S. T.; Hui, D.; Rahmat, L. K.; Fang, Q. *Compos. Part B: Eng.* **2013**, *47*, 238.
14. Fei, P.; Shi, Y.; Zhou, M.; Cai, J.; Tang, S.; Xiong, H. *J. Appl. Polym. Sci.* **2013**, *130*(6), 4129.
15. Li, Y.; Jiang, Y.; Liu, F.; Ren, F.; Zhao, G.; Leng, X. *Food Hydrocolloids* **2011**, *25*, 1098e1104.
16. Joost, U.; Juganson, K.; Visnapuu, M.; Mortimer, M.; Kahru, A.; Nommiste, E.; Joost, U.; Kisand, V.; Ivask, A. *J. Photochem. Photobiol. B: Biol.* **2015**, *142*, 178.
17. Melhem, H.; Di Bin, C.; Ratier, B.; Pardis, S.; Leconte, Y.; Herlin-Boime, N.; Janusik, M. M.; Kassiba, A.; Boucle, J. Photovoltaic technical Conference, PVTC 2012, 2012.
18. Zhang, L.; Bai, X.; Tian, H.; Zhong, L.; Ma, C.; Zhou, Y.; Chen, S.; Li, D. *Carbohyd. Polym.* **2012**, *89*(4), 1060.
19. Zhou, J. J.; Wang, S. Y.; Gunasekaran, S. *J. Food Sci.* **2009**, *74*(7), N50.
20. Yang, C.; Gong, C.; Peng, T.; Deng, K.; Zan, L. *J. Hazard. Mater.* **2010**, *178*.1, 152.
21. Wu, J. Y.; Li, C. W.; Tsai, C. H.; Chou, C. W.; Chen, D. R.; Wang, G. J. Synthesis of antibacterial $TiO_2$/PLGA composite biofilms [J]. *Nanomed: Nanotechnol. Biol. Med.* **2014**, *10*, 1097.
22. Xing, Y.; Li, X.; Zhang, L.; Xu, Q.; Che, Z.; Li, W.; Bai, Y.; Li, K. *Progr. Org. Coatings* **2012**, *73*(2), 219.
23. Gómez-Guillén, M. C.; Pérez-Mateos, M.; Gómez-Estaca, J.; Lopez-Gaballero, E.; Gimenez, B.; Montero, P. *Trends Food Sci. Technol.* **2009**, *20*(1), 3.
24. Zhang, T.; Zhou, P.; Zhan, Y.; Shi, X.; Lin, J.; Du, Y.; Li, X.; Deng, H. Pectin/lysozyme bilayers layer-by-layer deposited cellulose nanofibrous mats for antibacterial application [J]. *Carbohydrate polymers* **2015**, *117*, 687.
25. Singh, B. P.; Nayak, S.; Samal, S.; Bhattacharjee, S.; Besra, L. *Appl. Surf. Sci.* **2012**, *258*(8), 3524.
26. Kangwansupamonkon, W.; Lauruengtana, V.; Surassmo, S.; Ruktanonchai, U. *Nanomed. Nanotechnol. Biol. Med.* **2009**, *5.2*, 240.